Journal of
Instrumentation

Timepix4 spatial response characterization with X-ray monochromatic synchrotron beam

Published by IOP Publishing for Sissa Medialab

Received: *October 9, 2024*
Revised: *January 7, 2025*
Accepted: *January 26, 2025*
Published: *February 25, 2025*

25th International Workshop on Radiation Imaging Detectors
Lisbon, Portugal
30 June – 4 July 2024

Timepix4 spatial response characterization with X-ray monochromatic synchrotron beam

P. Delogu,[a,b] **N.V. Biesuz,**[d] **R. Bolzonella,**[c,d] **L. Brombal,**[e,f] **F. Brun,**[g,f] **P. Cardarelli,**[d] **V. Cavallini,**[c,d] **A. Feruglio**[h,b,*] **M. Fiorini,**[c,d] **R. Longo**[e,f] **and V. Rosso**[h,b]

[a] *Dipartimento di Scienze Fisiche, della Terra e dell'Ambiente, Università di Siena, Via Roma 56, Siena, 53100, Italy*
[b] *INFN Pisa, Largo Bruno Pontecorvo 3, Pisa, 56127, Italy*
[c] *Dipartimento di Fisica e Scienze della Terra, Università degli Studi di Ferrara, Via Saragat 1, Ferrara, 44122, Italy*
[d] *INFN Ferrara, Via Saragat 1, Ferrara, 44122, Italy*
[e] *Dipartimento di Fisica, Università degli Studi di Trieste, Via Valerio 2, Trieste, 34127, Italy*
[f] *INFN Trieste, Via Valerio 2, Trieste, 34127, Italy*
[g] *Dipartimento di Ingegneria e Architettura, Università degli Studi di Trieste, Via Valerio 10, Trieste, 34127, Italy*
[h] *Dipartimento di Fisica, Università di Pisa, Largo Bruno Pontecorvo 3, Pisa, 56127, Italy*

E-mail: alessandro.feruglio@phd.unipi.it

Abstract: The Timepix4 is a readout ASIC developed by the Medipix4 collaboration, designed to work with various semiconductor sensors to form detection systems with 448×512 pixels with a pitch of 55 µm. Its ability to simultaneously measure the Time of Arrival (ToA) and the Time over Threshold (ToT) of the signal makes it particularly suitable for spectral imaging applications. The ToT allows to measure the hit's energy, while the ToA enables to cluster the acquired events, recomposing the signal of the detected photons. The ability to cluster events allows to limit the degradation of the detector's spatial response caused by charge sharing effects, a common issue that affect conventional single-photon-counting detectors. This work aims to characterize the spatial response of a Timepix4-based detection system, in terms of the Edge Spread Function (ESF) and Line Spread Function (LSF), using a monochromatic X-ray beam. The characterization was performed at different energies (10 keV and 20 keV) using the moving edge method; different clustering methods were applied and compared during the analysis.

Keywords: X-ray detectors; Hybrid detectors; X-ray radiography and digital radiography (DR)

*Corresponding author.

https://doi.org/10.1088/1748-0221/20/02/C02047

2025 JINST 20 C02047

Contents

1 Introduction

Timepix4 [1] is a hybrid pixel detector readout ASIC of the Timepix family, developed by the Medipix4 collaboration [2]. It can be bump bonded to semiconductor sensors of different materials and thicknesses, composing a hybrid detection system of 448×512 pixels with a pitch of 55 µm. When a photon interacts with the sensor, electron-hole pairs are created and drifted by an electric field to the collection electrodes, where the collected charge is transferred to the pixels of the readout electronics. During the collection process charge sharing can occur and, due to electrons/holes diffusion, the signal of a single photon spreads across a cluster of pixels. Charge sharing is a limiting factor for the image quality of conventional single-photon-counting detectors, causing errors in the events counts and a degradation of the energy and spatial resolution of the devices [3]. Each pixel of the Timepix4 ASIC combines an analog front end and a digital section. The analog front end [4, 5] comprises an amplifier and a discriminator. When the input signal exceed the threshold, set above the noise level, the discriminator produces an output signal. The Timepix4 provides three operating modes: frame-based photon counting mode, data-driven photon counting mode and Time of Arrival (ToA) – Time over Threshold (ToT) data-driven mode. The latter allows the simultaneous measurement of the hits time of arrival and of the temporal length of each signal. After the system energy calibration, the ToT measures the energy released by the detected particles in each pixel. Using the information on ToA, it is possible to perform a clustering of the events: this operation, that groups pixels activated in the same radiation-sensor interaction, allows reconstructing the energy released by a single photon interacting in the sensor by summing the ToT signals of adjacent pixels with similar ToA. Moreover, by using different clustering methods it is possible to study the detector's intrinsic spatial resolution and to reduce effects of charge sharing.

In this work, a monochromatic X-ray beam was used to characterize the spatial response of the detection system by acquiring images of the sharp edge of a lead target. The data were processed

2025 JINST 20 C02047

by using different clustering methods to obtain some finely sampled Edge Spread Functions (ESFs). The ESFs have been analyzed with two different approaches to derive directly, in the first case, the finely sampled Line Spread Functions (LSFs) and analytically, in the second case, the pre-sampling LSFs. Data were acquired at two energies, 10 keV and 20 keV, to evaluate the system spatial response dependence on the energy.

2 Materials and methods

2.1 X-ray source

The data were acquired using the monochromatic X-ray beam of the SYRMEP (SYnchrotron Radiation for Medical Physics) beamline [6] of the Elettra Synchrotron in Trieste. The radiation is generated by a bending magnet of the storage ring and is filtered with a double-crystal Si (111) monochromator. The photon energy was selected by acting on the orientation of monochromator in the range 8.5 keV–40 keV, with an uncertainity on the monochromaticity $\Delta E/\mathrm{E} = 2 \cdot 10^{-3}$. The intensity of the beam was set by varying the relative angle of the crystals and applying Al filters, and it was monitored by a ionization chamber. The beam cross-section on the detector, defined by tungsten slits, was 5.2 mm (vertical) × 28.6 mm (horizontal). The vertical profile of the beam is Gaussian-like. In the following sections, to simplify the set-up representation in the images, the geometry of the system is rotated by 90°, and the SYRMEP laminar beam results as shown in figure 1.

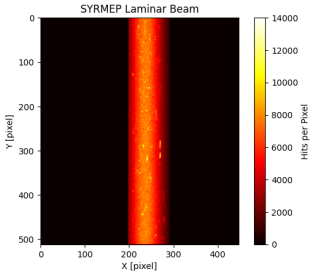

Figure 1. Laminar beam cross section on the detector. In the image, rotated by 90° with respect to the experimental conditions, the beam fully covers the detector extension in the vertical direction and 5.2 mm in the horizontal direction.

2.2 Measurement set-up

The acquisition were performed with a Timepix4_v2 ASIC bump-bonded to a 300 µm p-on-n Si sensor produced by Advafab [7], reverse biased at 100 V. The measurements were made in ToA-ToT data-driven mode. The detection threshold was set to 1000 e^- (3.6 keV); since this value is lower than the 50 % of the acquired X-rays energies, the signal produced by a single photon can exceed the threshold in multiple pixels and the effects of charge sharing can be analyzed. To stabilize the temperature of the detector at about 15° C, a custom cooling system, composed by a chiller and a copper heat exchanger, was implemented. The Timepix4 was connected to the computer with the SPIDR4 control board produced by Nikhef, with a 1 Gbps Ethernet cable for the device configuration and 2 fast link operating at 2.56 Gbps for the data readout. A custom made software was used to configure the system, acquire data and monitor the acquisitions. The detection system was energy

2025 JINST 20 C02047

calibrated [8–10]. A lead target with a sharp edge was placed in front of the detector, at about 5 mm from it. The target was moved by an hexapod motorized actuator with a minimum incremental step of 5 µm. This setup allowed the edge inclination to be fixed at 5 degrees relative to the pixel line.

2.3 Data acquisition

The aim of this work was to evaluate the intrinsic spatial response of the detection system using the moving edge method. Fifty images of a lead target with a sharp edge were acquired shifting the target position horizontally by steps of 5 µm (figure 2 (right). While the edge was shifted, four detectors pixels columns were gradually fully uncovered making it possible to finely study the detection system spatial response. About 15'000 hits per pixel were acquired for each position. To evaluate the spatial response of the detection system at different energies, acquisitions at 10 keV and at 20 keV were performed. A flat-field correction was applied to each image to adjust the Gaussian-like profile of the beam and its spatial non-uniformities.

2.4 Data analysis

Four different clusterization methods were employed in this work:

I non clustered events;

II clustered events, considering all cluster sizes events;

III clustered events, considering only size = 1 clusters;

IV clustered events, considering only size = 2 clusters parallel to the shift direction, the (a) case represented in figure 2 (right).

Before the events clustering (case I), charge-sharing generates hits in pixels adjacent to the one where the photon interacts, which degrades the spatial resolution of the system. By clustering the hits (case II), multiple counts are avoided, and the correct pixel to which the event should be assigned is determined by measuring the energy center of the cluster. Therefore, an improvement in the spatial resolution of the detector is expected in case II, which becomes more evident at higher energies where charge-sharing effects are more pronounced. Cases III and IV allow for studying the charge-sharing dependence on the photon interaction point within the pixel. A simple model of the pixel is shown in figure 2 (left). Photons that interact in the central region of the pixel (c) do not produce charge-sharing and result in single-pixel clusters (case III). Case III reproduces the behavior of a conventional single-photon-counting detector with the threshold set above 50% of photons energy, in which only single-pixel events are detected. The charge cloud produced by photons that interact in the lateral areas of the pixel (l) can be shared with the neighboring pixel, producing clusters of size two. Finally, photons interacting at the vertices of the pixels (v) can trigger hits in all neighboring pixels, generating clusters of size 3 or 4. These cases were not studied in this work due to the limited available statistics. As shown in figure 2 (right), size 2 clusters can be oriented either parallel to the direction of the edge motion (a) or perpendicular to it (b). Since the ESF is sampled in the direction of the edge motion, only the former were considered in case IV. These clusters represent only 4.9 % of total events at 10 keV and 15.5 % of the total events at 20 keV.

2025 JINST 20 C02047

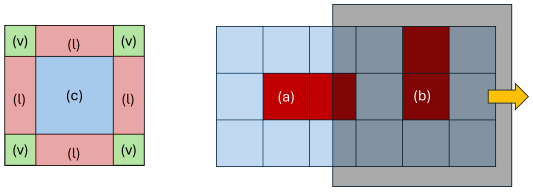

Figure 2. Left: charge-sharing model in the pixel: photons detected in the central area (c) do not produce charge sharing; the energy of the photons that impinge in pixel lateral regions (l) is shared only with one pixel; the energy of the photons that interact in pixel's vertices (v) can be shared with up to three other pixels. Right: cluster size = 2 events parallel (a) and perpendicular (b) to the direction of the edge motion. The edge is moved horizontally, as indicated by the yellow arrow in the figure.

2.4.1 Finely sampled ESFs

For each experimental condition and each clustering method, finely sampled ESFs were extracted from the edge images. Each of these is obtained as the counts measured in a pixel as the position of the target varies. In this context, the 5 µm shift of the target represents the sampling step of the ESF.

2.4.2 Direct method

To improve the statistical quality of the data, up to 100 different ESFs, extracted from different pixels, were combined to obtain a single, representative ESF. Then, the direct method involves directly differentiating the representative ESF. In this way, the LSF function is obtained with a sampling step of 5 µm. This direct method allows for evaluating the shape and measuring certain characteristics, such as the width, of the finely sampled LSF. The main advantage is that it does not require making prior assumptions about these characteristics. On the other hand, this method, since it involves direct differentiation on discrete data from photon counts, is very sensitive to statistical noise.

2.4.3 Analytical analysis

The analytical method involves fitting the finely sampled ESFs with analytical functions. These analytical functions are then differentiated to obtain the pre-sampled LSFs. Based on the results obtained with the direct method, two different analytical functions were chosen. For clustering of type I, II and III, the analytical ESF model is the convolution product [12]:

$$ESF(x) = R(x, x_0, k, m, M) * G(x, \sigma) \tag{2.1}$$

G(x, σ) is a normalized Gaussian function, R(x, x_0, k, m, M) is the linear ramp shown in figure 3 (left), that start in x_0 and rise between the minimum m and the maximum M with a slope k. The linear growth is related to the increase of the pixel surface exposed to radiation due to the edge shift.

Cluster of type IV are produced by events that interact in the lateral zones of the pixels. As shown in figure 3 (right), the ideal ESF is expected to be a double ramp function, rising at the two lateral sides of the pixel (zones A-C and D-B in figure 3) and remaining flat in the central area, where the charge cloud cannot trigger the two neighboring pixels. The ESF can therefore be described by the convolution product:

$$ESF(x) = DR(x, x0, k, m, M, L) * G(x, \sigma) \tag{2.2}$$

G(x, σ) is a normalized Gaussian function, DR(x, x_0, k, m, M, L) is the double ramp function, characterized by the L long flat region.

2025 JINST 20 C02047

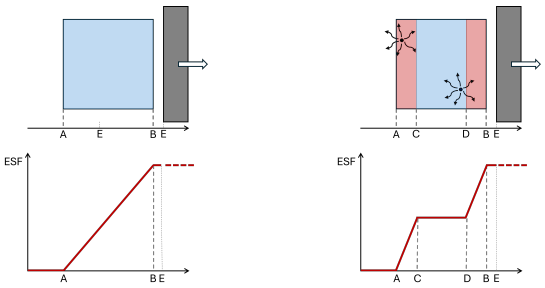

Figure 3. Ideal ESF for a square pixel considering all clustered events (left); ideal ESF for a square pixel considering only cluster size = 2 events with charge sharing in the direction perpendicular to the edge (right).

3 Results

3.1 Direct method

For each clustering method and energy, a representative ESF was obtained by averaging up to 100 single-pixel ESFs. Figure 4 shows, as an example, two finely sampled ESFs obtained for a single pixel by considering non-clustered events at 10 keV and 20 keV.

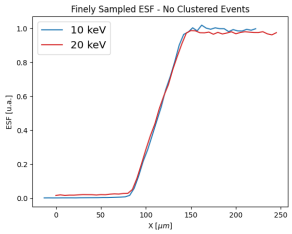

Figure 4. Example of finely sampled ESFs obtained for a single pixel considering non clustered events at 10 keV (blue) and 20 keV (red).

The LSFs, calculated by differentiating the representative ESFs, are shown in figure 5. The FWHM of the LSFs obtained using clustering methods I, II, and III are reported in table 1. The error associated with the results is half the sampling step. For the fourth clustering method, the LSFs present two peaks located in the A-C and D-B zones shown in figure 3 (right). To characterize this behaviour, the FWHM was measured on the individual peaks, resulting 12.0 ± 1.0 µm at 10 keV and 11.5 ± 1.0 µm at 20 keV. The results are discussed in section 3.3.

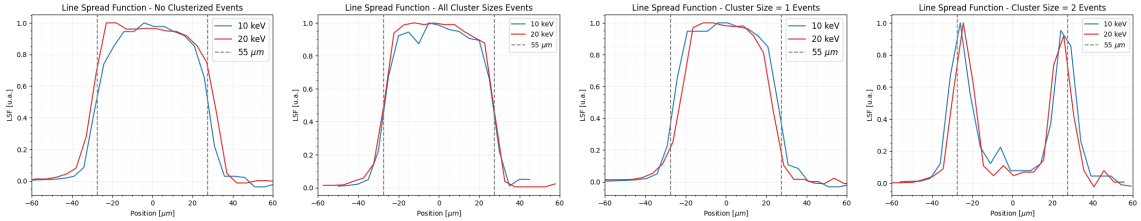

Figure 5. LSFs obtained, by direct measurement, for clustering methods I, II, III and IV at 10 keV (blue line) and 20 keV (red line). The dotted grey lines represent the 55 µm pixel pitch.

2025 JINST 20 C02047

Table 1. FWHM of the Line Spread Function calculated with the direct method.

		$FWHM_{10\,\mathrm{keV}}$ [µm]	$FWHM_{20\,\mathrm{keV}}$ [µm]
I	Non clustered events	56.7 ± 2.5	61.1 ± 2.5
II	All cluster sizes events	53.9 ± 2.5	54.4 ± 2.5
III	Cluster size = 1 events	51.7 ± 2.5	45.5 ± 2.5

3.2 Analytical analysis

For each energy, the finely sampled ESFs obtained for clustering method I, II, III were fitted with eq. (2.1) and the finely ESFs for clustering method IV were fitted with eq. (2.2). Figure 6 shows the results obtained at 10 keV for clustering method I (left) and IV (right) for a typical pixel. Due to lower available statistics, data acquired in case IV on a single pixel are subject to fluctuations, worsening the fit quality ($\chi^2 > 5$).

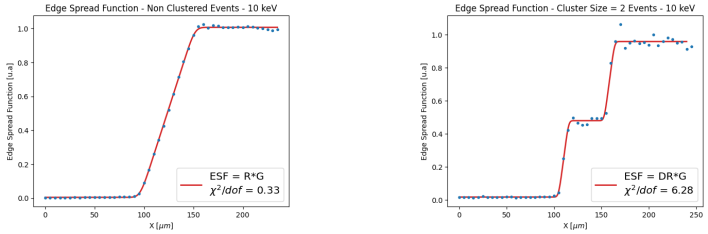

Figure 6. Left: example of ESF, obtained for a single pixel considering non clustered events at 10 keV, fitted with eq. (2.1). Right: example of ESF, obtained for a single pixel considering cluster size = 2 events at 10 keV, fitted with eq. (2.2).

Figure 7 shows the LSFs obtained by differentiating the finely sampled ESFs measured with the four clustering methods at 10 keV and 20 keV. The average FWHM of the LSFs, calculated for clustering methods I, II, and IV across fifteen pixels, is reported in table 2. For the fourth clustering method, the average FWHM of the individual peaks, calculated over fifteen pixels, is 11.8 ± 1.6 µm at 10 keV and 9.4 ± 2.7 µm at 20 keV. Results are discussed in section 3.3.

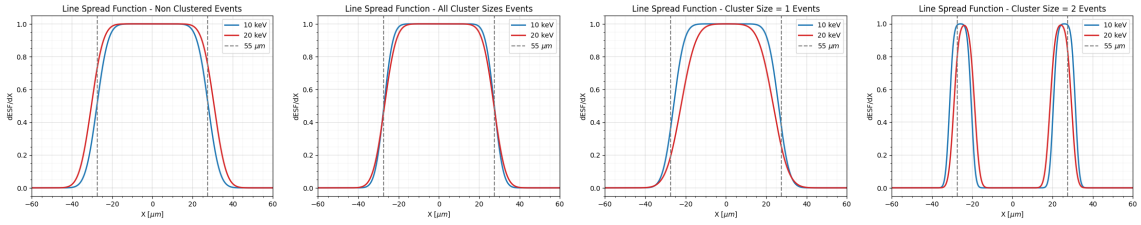

Figure 7. LSFs obtained, with the analytical analysis, for clustering methods I, II, III and IV at 10 keV (blue line) and 20 keV (red line). The dotted grey lines represent the 55 µpixel pitch.

3.3 Discussions

The results obtained from direct measurements, summarized in table 1, match those obtained from the analytical analysis, summarized in table 2. Without clusterization, the LSFs are slightly larger than the pixel pitch (55 µm) due to charge sharing. This effect is more pronounced at 20 keV than

2025 JINST 20 C02047

Table 2. Average FWHM of the Line Spread Function calculated with the analytical method.

		$FWHM_{10\,\mathrm{keV}}$ [µm]	$FWHM_{20\,\mathrm{keV}}$ [µm]
I	Non clustered events	55.5 ± 0.9	60.9 ± 0.9
II	All cluster sizes events	54.7 ± 1.3	54.3 ± 0.5
III	Cluster size = 1 events	51.9 ± 1.3	45.7 ± 1.0

at 10 keV, as the pixel area in which the interacting photons produce charge sharing above the fixed threshold (3.62 keV) is larger at higher energies. Thanks to clustering, the effects of charge sharing are corrected, and the photon interaction points are reconstructed by measuring the energy center of the clusters. In case II, the FWHM of the LSFs is, as expected, independent of energy and matches the pixel pitch. In case III, the LSFs are smaller than the pixel pitch, as only photons that interact in the central area of the pixel are considered. The LSF at 10 keV is larger since, at lower energies, photons that interact in the pixel's periphery can produce sub-threshold charge sharing, resulting in cluster size = 1 events. Finally, the LSFs observed in case IV confirm that events of cluster size = 2 correspond to photons that interact at the edges of the pixels, in an area approximately 10 µm wide.

4 Conclusions

In this work, the spatial response of a Timepix4 assembly equipped with a 300 µm thick silicon sensor has been characterized. The clusterization of events, performed using the ToA information, allows to limit the degradation of the detector spatial response, especially at higher energies where charge sharing is more impactful. After events clusterization the spatial resolution of the detection system results determined only to the pixel pitch (55 µm) both at 10 and 20 keV. The possibility to correct charge-sharing effects, which affects the spatial resolution of conventional single-photon counting detectors, demonstrate the potential of the Timepix4 for X-ray imaging applications. In particular, the high spatial resolution of the detector, combined with the capability to measure photons energy with a continuous spectrum, makes the Timepix4 particularly suitable for spectral imaging applications. Finally, the correspondence between the qualitative and quantitative results obtained with the direct measurement and with the analytical model validates the two functions introduced to describe the ESF. These models can therefore be used to describe the spatial response of the detector and allow to accurately reproduce the charge sharing effects in Monte Carlo simulations of the detector.

Acknowledgments

This work was carried out in the context of the Medipix4 Collaboration based at CERN, and partially supported by the MEDIPIX4 project funded by the INFN (Italian Institute for Nuclear Physics), CSN5 (National Scientific Commission 5). We acknowledge Elettra Sincrotrone Trieste for providing access to its synchrotron radiation facilities and for financial support under the IUS internal project.

References

[1] X. Llopart et al., *Timepix4, a large area pixel detector readout chip which can be tiled on 4 sides providing sub-200 ps timestamp binning*, 2022 *JINST* **17** C01044.

[2] Medipix4, https://medipix.web.cern.ch/medipix4 [accessed 2024-03-26].

[3] V. Di Trapani et al., *Characterization of the acquisition modes implemented in Pixirad-1/Pixie-III X-ray Detector: Effects of charge sharing correction on spectral resolution and image quality*, *Nucl. Instrum. Meth. A* **955** (2020) 163220.

[4] R. Ballabriga et al., *The Timepix4 analog front-end design: Lessons learnt on fundamental limits to noise and time resolution in highly segmented hybrid pixel detectors*, *Nucl. Instrum. Meth. A* **1045** (2023) 167489.

[5] K. Heijhoff et al., *Timing performance of the Timepix4 front-end*, 2022 *JINST* **17** P07006 [arXiv:2203.15912].

[6] G. Tromba et al., *The SYRMEP Beamline of Elettra: Clinical Mammography and Bio-medical Applications*, *AIP Conf. Proc.* **1266** (2010) 18.

[7] Medipix4, https://advafab.com/ [accessed 2024-04-22].

[8] P. Delogu et al., *Validation of Timepix4 energy calibration procedures with synchrotron X-ray beams*, *Nucl. Instrum. Meth. A* **1068** (2024) 169716.

[9] A. Feruglio et al., *Timepix4 characterization with monochromatic X-rays at the Elettra synchrotron facility*, *Nucl. Instrum. Meth. A* **1069** (2024) 169844.

[10] A. Feruglio et al., *Timepix4 calibration and energy resolution evaluation with fluorescence photons*, *Nuovo Cim. C* **47** (2024) 314.

[11] P. Delogu et al., *Characterization of Pixirad-1 photon counting detector for X-ray imaging*, 2016 *JINST* **11** P01015.

[12] H.T. Philipp et al., *Very-High Dynamic Range, 10,000 Frames/Second Pixel Array Detector for Electron Microscopy*, *Microscopy Microanal.* **28** (2022) 425 [arXiv:2111.05889].

2025 JINST 20 C02047